Mathematical Simulation of Behavior of Carbon and Oxygen in RH Decarburization

Peng-huan LI, Qiao-jun WU, Wen-hao HU, Jian-song YE
(Hangzhou Iron & Steel Group Company, Hangzhou 310022, Zhejiang, China)

Abstract: A mathematical model for RH decarburization was developed on the basis of the principle of carbon and oxygen balance. In the simulation, a physical description of the different reaction sites associated with the different mechanisms was considered. Furthermore, the oxygen transfer between top slag and molten steel was also considered. The calculated results of the model were in good agreement with the operation data of the two different plants. The model was applied to analyze the effect of KTB starting time on the RH decarburization rate for ultra-low carbon steel production using slag reforming or LF refining. According to the results, the RH decarburization rate especially the inner site decarburization rate is controlled by the KTB starting time. In actual operation, late KTB starting time should be avoided.

Key words: RH decarburization; vacuum refining; numerical simulation; ladle top slag

Symbol List

α—Constant, $\alpha=4/3(D_O/D_C)^{0.5}$;
a_{FeO}—Activity of FeO;
$a_{FeO(RS)}$—Activity of FeO calculated by regular model;
A_i—Reaction surface, m^2;
C_i—Carbon content in interface, 10^{-6};
$C_{E,i}$—Equilibrium carbon content in interface, 10^{-6};
C_L, C_V—Carbon content in molten steel in ladle and vessel, 10^{-6};
FeO_S—FeO content in slag related to mass of steel, mass%;
g—Acceleration of gravity, $m\cdot s^{-2}$;
G—Ar gas flowrate, $L\cdot min^{-1}$;
$O_{E,i}$—Equilibrium oxygen content in interface, 10^{-6};
O_L, O_V—Oxygen content in molten steel in ladle and vessel, 10^{-6};
H_{CO}—Depth of CO formation region, m;
$K_{C,i}$—Transfer coefficient of carbon, $m\cdot s^{-1}$;
K_V—Volumetric coefficient for decarburization as CO bubbles, $\%\cdot(Pa\cdot s)^{-1}$;
K_{CO}—Equilibrium constant of interfacial reaction, $Pa\cdot\%^{-2}$;
M_C, M_O—Molecular mass of C and O, $g\cdot mol^{-1}$;
M_{FeO}—Molecular mass of FeO, $g\cdot mol^{-1}$;
n_{CO}—Amount of CO in a bubble, mol;
$n_{CO,r}$—Amount of CO absorbed by rising Ar bubbles, mol;
O_{LQ}—Equilibrium oxygen content in ladle, 10^{-6};
$P_{CO,i}$—Partial pressure in interface, Pa;
P_V—Vessel pressure, Pa;
Q—Steel circulation rate, $t\cdot min^{-1}$;
RO_{Slag}—Oxygen transfer rate between top slag and molten steel, $10^{-6}\ s^{-1}$;
RO_{KTB}—Supply oxygen rate of KTB, $10^{-6}\ s^{-1}$;
t—Time, s;
T—Molten steel temperature, K;
T_{OL}—Reaction time constant for FeO reduction, s;
W_L, W_V—Mass of molten steel in ladle and vessel, t;
W_{Slag}—Mass of top slag, kg;
X_{FeO}—Mole fraction of FeO;
ρ—Density of steel, $t\cdot m^{-3}$;
γ_{FeO}—Activity coefficient of FeO;
τ—Time required for Ar bubble away from the nozzle to the bath surface, s;
ΔC_i—Decarburization amount of Ar bubbles, bath surface and inner site, $g\cdot s^{-1}$;
ΔO_i—Deoxidation amount of Ar bubbles, bath surface and inner site, $g\cdot s^{-1}$;
Subscript
i—Decarburization site, i=Ar, Surface, Inner.

According to the chemical reaction rule, the theoretical ratio of decarburization amount and deoxidation amount conforms to the stoichiometric relation of 3/4. However, the actual drop amount does not accord with the above stoichiometric relation. Dunkirk Steel Company of French showed that the actual ratio was about 1.1[1]. Yamaguchi et al.[2] found that oxygen transfer rate was mainly affected by the TFe content of the ladle slag in RH decarburization. These facts indicate that the oxygen transfer occurs between top slag and steel in RH decarburization, thereby affects the steel oxygen content and decarburization reaction. There are many studies on RH decarburization simulation, but most studies only focus on the simulation of carbon content and ignore the

Biography: Peng-huan LI, Doctor, Senior Engineer; **E-mail:** lipenghuan2010@163.com

simulation of oxygen content and the impact of top slag on RH decarburization[3-12]. Therefore, developing a RH decarburization model is of great significance, which involves mass balance, location of decarburization, and oxygen transfer between top slag and molten steel.

1 Mathematical Model

1.1 Basic assumptions

The model applies the following assumptions:

(1) Reaction sites include the Ar bubbles, bath surface and CO bubbles formation at inner site.

(2) The molten steel is perfectly mixed in both ladle and vacuum vessel.

(3) The rate of decarburization is controlled by the mass transfer of carbon and oxygen.

(4) The carbon and oxygen concentration at the gas-metal interface is in equilibrium with the partial pressure of CO in the gas phase.

(5) Bubbles are global and do not coalesce.

(6) Equilibrium reaction between molten steel and slag occurs: [Fe]+[O]=(FeO).

1.2 Basic equations

The mass balance of carbon and oxygen in the ladle and the vacuum vessel is represented by Eqs. (1) to (4).

$$W_{\mathrm{L}}\frac{\mathrm{d}C_{\mathrm{L}}}{\mathrm{d}t}=Q(C_{\mathrm{V}}-C_{\mathrm{L}}) \tag{1}$$

$$W_{\mathrm{L}}\frac{\mathrm{d}O_{\mathrm{L}}}{\mathrm{d}t}=Q(O_{\mathrm{V}}-O_{\mathrm{L}})+W_{\mathrm{L}}RO_{\mathrm{Slag}} \tag{2}$$

$$W_{\mathrm{V}}\frac{\mathrm{d}C_{\mathrm{V}}}{\mathrm{d}t}=Q(C_{\mathrm{L}}-C_{\mathrm{V}})-(\Delta C_{\mathrm{Ar}}+\Delta C_{\mathrm{Surface}}+\Delta C_{\mathrm{Inner}}) \tag{3}$$

$$W_{\mathrm{V}}\frac{\mathrm{d}O_{\mathrm{V}}}{\mathrm{d}t}=Q(O_{\mathrm{L}}-O_{\mathrm{V}})-(\Delta O_{\mathrm{Ar}}+\Delta O_{\mathrm{Surface}}+\Delta O_{\mathrm{Inner}})+W_{\mathrm{V}}RO_{\mathrm{KTB}} \tag{4}$$

The relation between carbon concentration and oxygen concentration at the gas-metal interface is expressed by Eq. (5).

$$\log(10^{-8}C_{\mathrm{E,i}}O_{\mathrm{E,i}}/P_{\mathrm{CO,i}})=-(1\,160/T+2.003) \tag{5}$$

The ratio of decarburization and deoxidation amount of each site satisfies the stoichiometric ratio, as shown in Eq. (6).

$$(\Delta O_{\mathrm{Ar}}+\Delta O_{\mathrm{Surface}}+\Delta O_{\mathrm{Inner}})=\frac{M_{\mathrm{O}}}{M_{\mathrm{C}}}(\Delta C_{\mathrm{Ar}}+\Delta C_{\mathrm{Surface}}+\Delta C_{\mathrm{Inner}}) \tag{6}$$

(1) Decarburization through Ar bubbles

The rate of the chemical reaction at the bubble interface is as follows.

$$\frac{\mathrm{d}n_{\mathrm{CO}}}{\mathrm{d}t}=A_{\mathrm{Ar}}K_{\mathrm{C,Ar}}\frac{\rho}{M_{\mathrm{C}}}(C_{\mathrm{V}}-C_{\mathrm{E,Ar}}) \tag{7}$$

The $C_{\mathrm{E,Ar}}$ is expressed by Eq. (8).

$$C_{\mathrm{E,Ar}}=\{(\alpha C_{\mathrm{V}}-O_{\mathrm{V}})+[(\alpha C_{\mathrm{V}}-O_{\mathrm{V}})+4\alpha P_{\mathrm{CO,Ar}}\cdot 10^{5.997-1\,160/T}]^{1/2}\}/2\alpha \tag{8}$$

The amount of substance of CO absorbed by rising Ar bubbles can be expressed as

$$\sum n_{\mathrm{CO,r}}=\int_0^{\tau}\frac{\mathrm{d}n_{\mathrm{CO}}}{\mathrm{d}t}\mathrm{d}t \tag{9}$$

The decarburization rate of Ar bubbles can be expressed as

$$\Delta C_{\mathrm{Ar}}=M_{\mathrm{C}}\sum n_{\mathrm{CO,r}}/\tau \tag{10}$$

(2) Decarburization through free surface in a vacuum vessel

$$\Delta C_{\mathrm{Surface}}=(A_{\mathrm{Surface}}\cdot\rho)\cdot K_{\mathrm{C,Surface}}\cdot(C_{\mathrm{V}}-C_{\mathrm{E,Surface}}) \tag{11}$$

The $C_{\mathrm{E,Surface}}$ is expressed by Eq. (12).

$$C_{\mathrm{E,Surface}}=\{(\alpha C_{\mathrm{V}}-O_{\mathrm{V}})+[(\alpha C_{\mathrm{V}}-O_{\mathrm{V}})^2+4\alpha P_{\mathrm{CO,\,Surface}}\cdot 10^{5.997-1\,160/T}]^{1/2}\}/2\alpha \tag{12}$$

(3) Decarburization as CO bubbles

The decarburization rate as CO bubbles is expressed by Eq. (25) on the assumption that CO formation is proportional to the super saturation.

$$-\frac{\mathrm{d}C_{\mathrm{Inner}}}{\mathrm{d}t}=K_{\mathrm{V}}(K_{\mathrm{CO}}w_{[\mathrm{C}]}w_{[\mathrm{O}]}-P_{\mathrm{V}}) \tag{13}$$

The volumetric coefficient for the decarburization as CO bubbles should be changed with the depth of the CO bubble formation region. A basic volumetric coefficient k_{O} is determined by depth h_{O}, and K_{V} is calculated by Eq. (15). The basic coefficient k_{O} is determined by the trial and error method from the comparison of calculations with the real data.

$$H_{\mathrm{CO}}=(K_{\mathrm{CO}}w_{[\mathrm{C}]}w_{[\mathrm{O}]}-P_{\mathrm{V}})/\rho g \tag{14}$$

$$K_{\mathrm{V}}=k_{\mathrm{O}}\times H_{\mathrm{CO}}/h_{\mathrm{O}} \tag{15}$$

The decarburization rate of inner sites can be expressed as

$$\Delta C_{\mathrm{Inner}}=10^4\cdot K_{\mathrm{V}}(101\,325\cdot K_{\mathrm{CO}}C_{\mathrm{V}}O_{\mathrm{V}}\cdot 10^{-8}-P_{\mathrm{V}}) \tag{16}$$

(4) The oxygen transfer rate between top slag and molten steel

The activity of FeO is important in calculating the oxygen transfer rate between top slag and molten steel. In Kleimt's model, the activity of FeO is assumed to be its mole fraction in the slag, which is easier for calculation but not accurate[13]. In present model, regular solu-

tion model is used to calculate the activity of FeO which proves to be useful and correct[14,15].

For simplification, it is assumed that only FeO is reduced. According to the regular solution model, the activity of FeO in slag can be calculated as follows

$$a_{\mathrm{FeO(RS)}} = \gamma_{\mathrm{FeO}} X_{\mathrm{FeO}} \tag{17}$$

$$a_{\mathrm{FeO}} = 0.864 a_{\mathrm{FeO(RS)}} \tag{18}$$

The oxygen transfer rate between top slag and molten steel is written as

$$RO_{\mathrm{Slag}} = \frac{1}{T_{\mathrm{OL}}}(O_{\mathrm{LQ}} - O_{\mathrm{L}}) \tag{19}$$

The FeO reduction is itself described by a first order differential equation for FeOs.

$$-\frac{\mathrm{d}(FeO_{\mathrm{S}})}{\mathrm{d}t} = \frac{M_{\mathrm{FeO}}}{M_{\mathrm{O}}} \frac{W_{\mathrm{L}}}{W_{\mathrm{Slag}}} RO_{\mathrm{Slag}} \cdot 10^4 \tag{20}$$

2 Results and Discussion

2.1 Model validation

With two different processes of plant A and B, the experimental data is obtained to verify the established model. Plant A produces ultra-low carbon steel with traditional BOF-RH-CC process, and top slag is modified before RH. While plant B applies LF refining before RH in order to ensure castability for its ASP casting machine. The parameters of RH equipment are shown in Table 1. The initial composition of molten steel and top slag is shown in Table 2.

Actual measured data is applied to RH vacuum vessel pressure, which is shown in Fig. 1. For plant B, pre-vacuum and a pressure drop platform of 8 000 Pa for a certain period is adopted. According to stoichiometry, the initial oxygen content of 2 heats does not satisfy the RH decarburization. Therefore, KTB blowing operations are carried out, of which specific parameters are shown in Fig. 2.

Calculated values conform to measured ones perfectly, as shown in Fig. 3, which means that the model is feasible.

Table 1 Dimensions of the RH system

Parameter	A	B
Heat size/t	300	150
Inside diameter of vacuum vessel/m	2.65	1.80
Inside diameter of snorkel/m	0.75	0.50

Table 2 RH initial steel and slag composition

No.	Steel composition/10^{-6}		Slag composition/mass%						
	[C]	[O]	Al_2O_3	CaO	MgO	MnO	P_2O_5	SiO_2	FeO
A	382	370	26.98	54.74	5.62	0.97	0.42	7.62	3.64
B	390	10	32.30	51.92	7.13	0.28	0.03	7.88	0.47

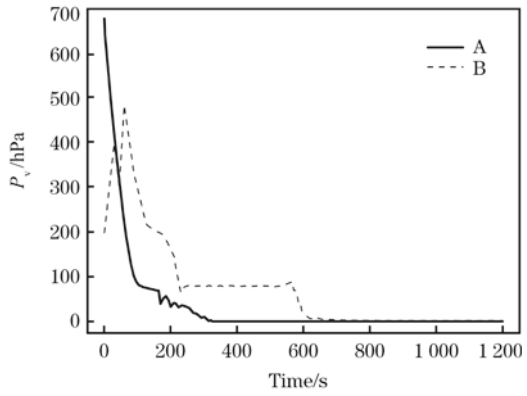

Fig. 1 Pressure variation of vacuum vessel

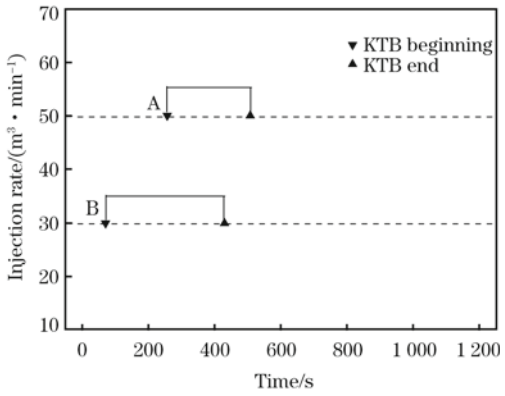

Fig. 2 KTB blowing mode

2.2 The effect of KTB on RH decarburization

KTB starting time is important if the dissolved oxygen in steel is insufficient. As shown in Fig. 2, the KTB starting time is proper for plant B, while relatively lagged for plant A. A typical heat, of which KTB starting time seriously lagged, is selected to be analyzed. The carbon and oxygen content of molten steel is 446×10^{-6} and 445×10^{-6} at the beginning of RH refining. The KTB

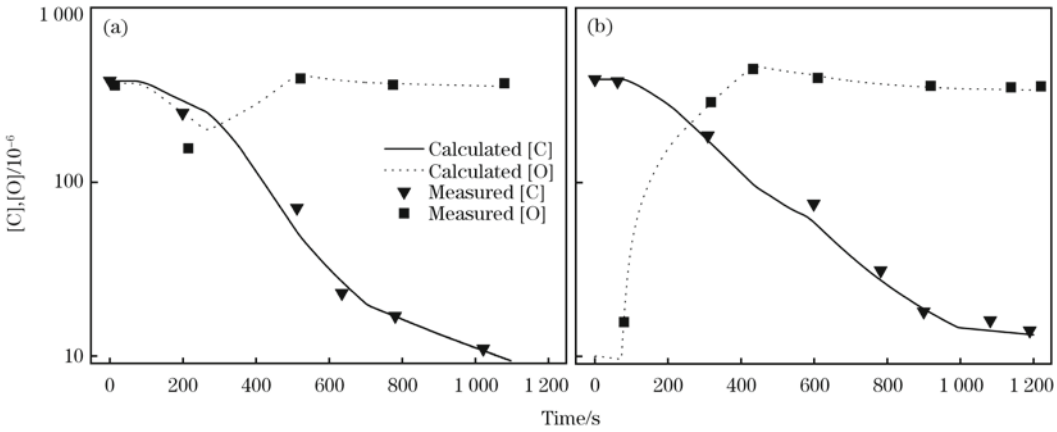

Fig. 3 The model calculated and measured values for plant A (a) and plant B (b)

operating parameters are shown in Table 3, and the model results are shown in Fig. 4.

For this heat, the stoichiometric shows that the oxygen content requires 575×10^{-6} if the carbon content drops to 15×10^{-6}. Thus, the initial oxygen content does not meet the demand of RH decarburization.

Table 3 KTB process control parameters

Start time/s	387
End time/s	758
Injection rate/($m^3\cdot min^{-1}$)	50

As Fig. 4(a) shows, RH decarburization mainly depends on inner decarburization. For this heat, inner decarburization rate experiences a rapid decline after a short peak, and a stagnation zone as long as 2 min appears before KTB starting, as shown in the box area. As KTB starting time is seriously lagged, the oxygen content before KTB has suffered severe loss, and the depth of CO bubble formation area continues to decrease, which leads to the decrease of inner decarburization rate.

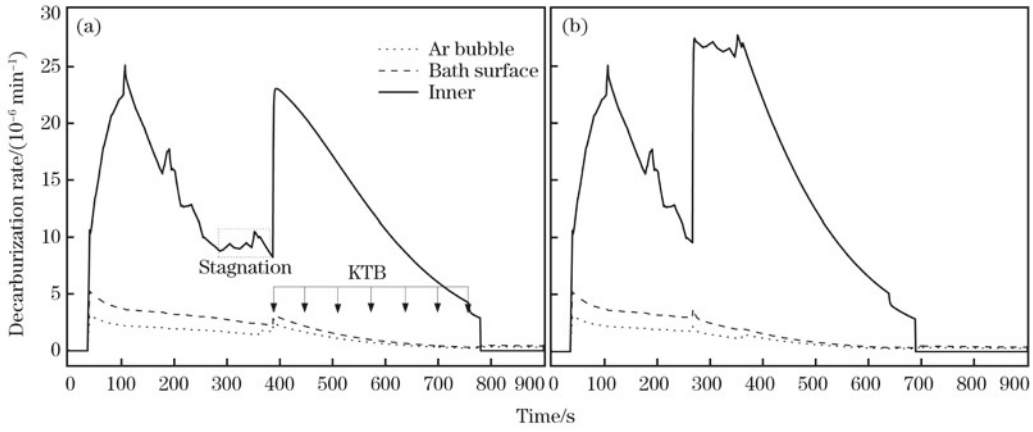

(a) Original; (b) Improved.

Fig. 4 Decarburization rate curve

Maintaining the blowing rate and KTB total time constant and starting KTB blowing ahead of 2 min are applied to the improved oxygen process. The decarburization rates of different sites of the improved process are shown in Fig. 4(b).

As Fig. 4(a) shows, the stagnation region of inner decarburization rate disappears and maintains a certain period at the peak after KTB starts. Therefore, earlier KTB is important to improve RH decarburization rate.

3 Conclusions

A RH carbon-oxygen reaction model is established, which involves mass balance, location of decarburization reaction, and oxygen transfer between top slag and molten steel. The model accurately forecasts the carbon and

oxygen content in the steel during RH decarburization.

For the heats of which oxygen is insufficient for the demand of decarburization, the decarburization rate will decrease significantly if KTB starting time is lagged, especially the inner decarburization rate shows a stagnation region.

References:

[1] M. Nadif, D. Brachet, in: 1989 Steelmaking Conference Proceedings, Chicago, 1989, pp. 227-233.

[2] K. Yamaguchi, Y. Kishimoto, T. Sakuraya, T. Fujii, M. Aratani, H. Nishikawa, ISIJ Int. 32 (1992) 126-135.

[3] K. Uemura, M. Takahashi, S. Koyama, Kobe Steel Eng. Rep. 41 (1991) No.4, 24-27.

[4] S. Kitamura, M. Yano, K. Harashima, N. Tsutsumi, Tetsu-to-Hagané 80 (1994) No.3, 213-218.

[5] M. Takahashi, H. Matsumoto, T. Saito, ISIJ Int. 35 (1995) 1452-1458.

[6] T. Kitamura, K. Miyamoto, R. Tsujino, S. Mizoguchi, K. Kato, ISIJ Int. 36 (1996) 395-401.

[7] H. Saint-Raymond, D. Huin, F. Stouvenot, Mater. Trans. JIM 41 (2000) No.1, 17-21.

[8] J. H. Wei, N. W. Yu, Steel Res. Int. 73 (2002) No.4, 135-142.

[9] Y. G. Park, K. W. Yi, ISIJ Int. 43 (2003) 1403-1409.

[10] M. Y. Zhu, Y. L. Wu, C. W. Du, Z. Z. Huang, J. Iron Steel Res. Int. 12 (2005) No.2, 20-24.

[11] J. M. Zhang, L. Liu, X. Y. Zhao, S. W. Lei, Q. P. Dong, ISIJ Int. 54 (2014) 1560-1568.

[12] S. Y. Kitamura, H. Aoki, K. I. Miyamoto, H. Furuta, K. Yamashita, K. Yonezawa, ISIJ Int. 40 (2000) 455-459.

[13] B. Kleimt, S. Kohle, H. J. Ponten, W. Matissik, D. Schewe, Ironmak. Steelmak. 20 (1993) 390-395.

[14] B. Y. Shiro, ISIJ Int. 33 (1993) 2-11.

[15] S. H. Kim, B. Song, Metall. Mater. Trans. B 33 (1999) 435-442.